Dehydration of Water–Alcohol Mixtures by Vapor Permeation Through PVA/Clay Nanocomposite Membrane

Jui-Ming Yeh, Ming-Yao Yu, Shir-Joe Liou

Department of Chemistry and Center for Nanotechnology, Chung-Yuan Christian University, Chung Li, Taiwan 320, Republic of China

Received 15 July 2003; accepted 6 December 2002

ABSTRACT: An organic/inorganic hybrid nanocomposite membrane, poly(vinyl alcohol)/clay (PVAC), was prepared. The morphology of PVAC nanocomposite membranes were characterized using transmission electron microscopy (TEM), X-ray diffraction (XRD), and atomic force microscopy (AFM). The crystallinity and surface roughness increases with an increasing clay content in the PVAC nanocomposite membrane. Compared with the pure poly(vinyl alcohol) (PVA) membrane, the hybrid nanocomposite membrane (PVAC) shows an improvement in the thermal stability and the prevention of the water-soluble property. The oxygen permeability and the water-vapor permeation rate decreases with an increasing clay content (1–3 wt %) in the PVAC nanocomposite membranes. In addition, the effects of the clay content on the vapor-permeation performance of an aqueous ethanol solution through the PVAC nanocomposite membranes was also investigated. © 2003 Wiley Periodicals, Inc. J Appl Polym Sci 89: 3632–3638, 2003

Key words: clay; nanocomposite; poly(vinyl alcohol); permeation

INTRODUCTION

Dehydration of alcohol is one of the important developed areas of vapor-permeation and pervaporation separation processes. The key to success of the pervaporation process is that, if suitable membranes can be fabricated, high permeability, good selectivity, and proper mechanical strength are the criteria for choosing suitable vapor-permeation and pervaporation membranes. Thus, synthesizing new polymeric materials with good pervaporation and vapor-permeation performance is exceedingly important. Poly(vinyl alcohol) (PVA) is one of the most widely used polymer materials for membrane-separation technology. However, the abundant hydrophilicity moiety in the polymer chain induced an excessive swelling during the pervaporation process. Therefore, a modified hydrophilic membrane was developed to avoid this excessive swelling. Thus, many researchers have focused their attention on improving the stability of PVA through a physical and chemical crosslinking reaction.[1,2] However, because organic feed mixtures are directly in contact with polymer membranes in the pervaporation process, the physical and chemical properties of the membranes are often influenced by the feed mixtures via effects of swelling or shrinking on the membranes.

Accordingly, to enhance the permselectivity of the polymer membranes for an aqueous organic solution, it is very important to control the swelling or shrinking of the membranes. Vapor permeation, a membrane-separation technique, was proposed by Uragami et al.[3,4] to improve the disadvantages of pervaporation. In this vapor-permeation technique, the feed solution was vaporized first and then permeated through the membrane. Thus, the swelling or shrinking of polymer membranes due to the feed solutions can be prevented. Recently, the preparation of organic/inorganic hybrid materials has attracted research interest. A polymer nanocomposite is a hybrid material composed of an organic polymer matrix in which inorganic material with nanoscale dimensions are dispersed.[5] The inorganic materials improve the physical and mechanical properties of a polymer. The polymer nanocomposite exhibits higher heat-distortion temperatures, a decreased thermal-expansion coefficient, and better barrier properties.[6] The enhanced properties are presumably due to the effects of the nanoscale structure and the interaction between the organic and inorganic materials. For this reason, there has been increased interest in its use. The purpose of this work was to study the effects of the clay content on the properties of PVAC nanocomposite materials. In addition, the effects of the clay content on the vapor-permeation performances of an aqueous ethanol solution through PVAC nanocomposite membranes were also investigated.

EXPERIMENTAL

Materials

A Na^+-type montmorillonite (pk-805) with a cation-exchange capacity of 95 meq/100 g was supplied by

Correspondence to: J.-M. Yeh.

Journal of Applied Polymer Science, Vol. 89, 3632–3638 (2003)

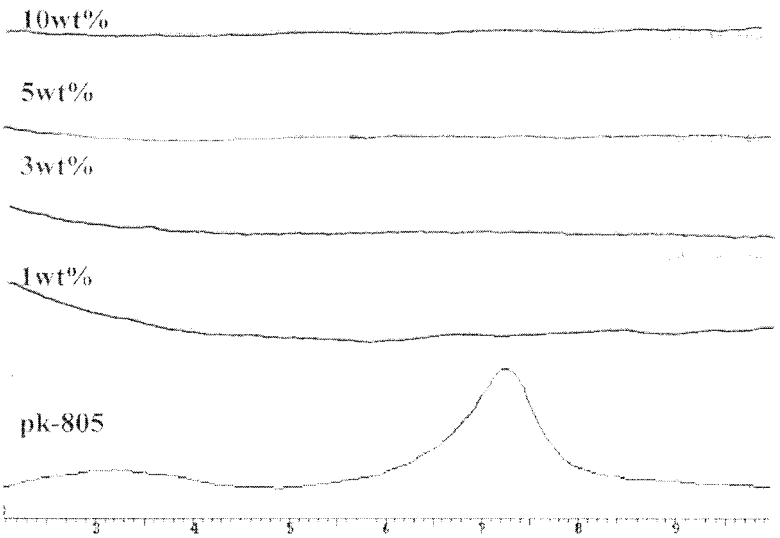

Figure 1 X-ray diffraction patterns of nanocomposite materials.

the Industrial Technology Research Institute (ITRI). PVA (BF-14, viscosity = 12–16 cps, hydrolysis = 98.5–99.2 mol %) was supplied by the Chang Chun Petrochemical Co. Ltd. Ethanol (R.D.H.) and CH_2Cl_2 (Merck) were of reagent grade. Water was deionized and distilled.

Poly(vinyl alcohol)/clay (PVAC) nanocomposite membrane preparation

PVAC nanocomposite membranes were prepared from a 7.5 wt % (PVA/H_2O) casting solution with varying compositions of clay added. Casting the solution onto a glass plate to a predetermined thickness using a Gardner knife formed the membrane. The glass plate was then heated at 70°C for 1 h. Then, the membrane was peeled off and dried in a vacuum for 24 h. The average membrane thickness was about 50 μm.

Characterization

Wide-angle X-ray diffraction scans were generated by a Rigaku D/MAX-3C OD-2988N diffractometer using a Ni-filtered CuKα target at a scanning rate of 4°C/min. Fourier transform infrared (FTIR) spectra were recorded on a Perkin–Elmer spectrum. Thermogravimetric data and differential scanning calorimetry analysis were obtained on a Perkin–Elmer TGA-7 and DSC-7 thermal analysis system in flowing nitrogen (60

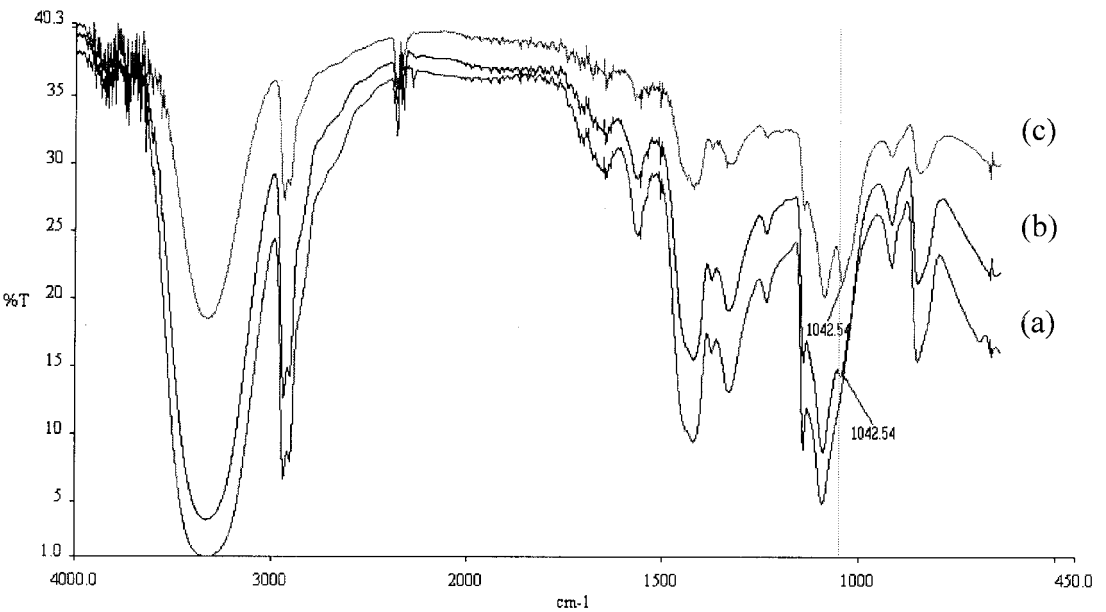

Figure 2 FTIR spectra of the PVAC nanocomposite membranes: (a) PVA; (b) PVAC3; (c) PVAC10.

Figure 3 TEM photograph of PVAC10.

cm^3/min) at a heating rate of 20°C/min. The membrane structures were examined by a JEOL-200FX transmission electron microscope (TEM) with an acceleration voltage of 120 kV and an atomic force microscope (AFM) (Digital Instrument, DI-NSIIIa) in the tapping mode.

Gas-permeability measurement

Oxygen permeabilities of membranes were determined using a Yanco GTR-10 gas-permeability analyzer. The gas permeability was measured by the following equation:

$$P = \frac{l}{(p1 - p2)} \frac{q/t}{A}$$

where P is the gas permeability [cm^3(STP) cm cm^{-2} s^{-1} $cmHg^{-1}$]; q/t, the volume flow rate of the gas permeate [cm^3(STP)/s]; l, the membrane thickness (cm); A, the effective membrane area (cm^2); and $p1$ and $p2$, the pressures (cmHg) on the high-pressure and low-pressure sides of the membrane, respectively.

Vapor-permeation measurement

A traditional vapor-permeation process was used.[7] The feed vapor is in direct contact with the membrane with an effective area of 7.06 cm^2. In this experiment, the permeation rate was measured the weight of the permeate. A vacuum pump maintained the downstream pressure at 3–5 mmHg. The permeation rate was determined by

$$P = W/(A \times t) \text{ (g } m^{-2}h^{-1})$$

where P, W, A, and t represent the permeation rate (g m^{-2} h^{-1}), the weight of the permeate (g), the effective membrane area (m^2), and the operation time (h), respectively. The composition of the permeate was measured by gas chromatography (GC; China chromatograph 8700T). The separation factor was calculated from

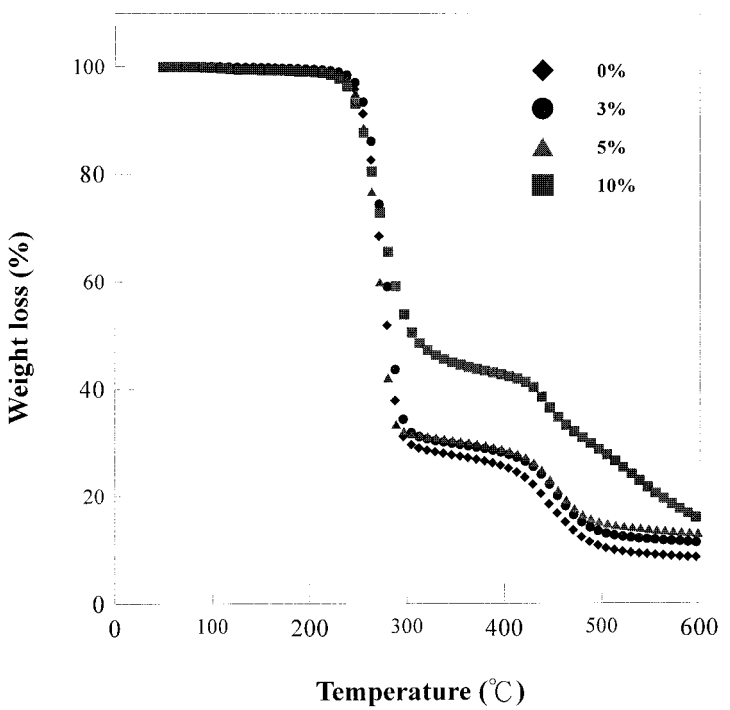

Figure 4 TGA curves of the PVAC nanocomposite materials.

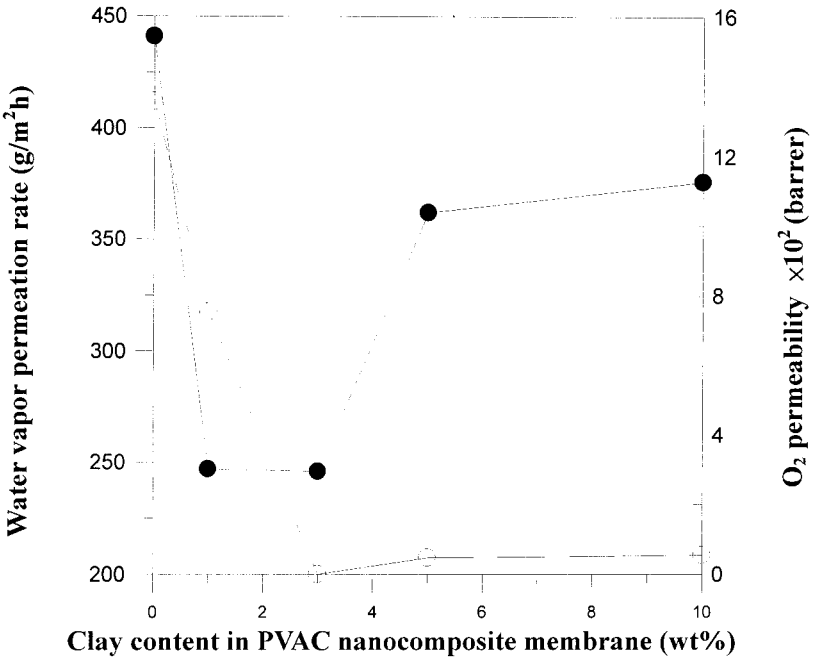

Figure 5 Effect of clay content on the (○) oxygen permeability (barrer) and (●) water-permeation rate (g m^{-2} h^{-1}).

$$\alpha_{A/B} = (Y_A/Y_B)/(X_A/X_B)$$

where X_A/X_B and Y_A/Y_B are the weight fractions of A and B of water and alcohol vapors in the feed and permeate; especially, A was the more permeative species. The average results were repeatedly measured four times in each condition. The data error was in the range of ±10%.

Contact-angle measurements

The contact angle of CH_2Cl_2 was measured with a face contact-angle meter CA–D type (Kyowa Interface Science Co. Ltd.). Sets of droplets (sessile drop; volume of approximately1.8 × 10^{-3} cm^3) of water were placed on a membrane-covered fixing knob. The dimensions of the droplets were measured approximately 10 s after placing the droplets on the knob. The droplets must be small enough so that their shape approximates a sphere. The contact angle was calculated by the following condition:

$$\text{Contact angle} = 2\tan^{-1}(h/r)$$

where h is the height of the spherical segment, and r, the radial of the spherical segment.

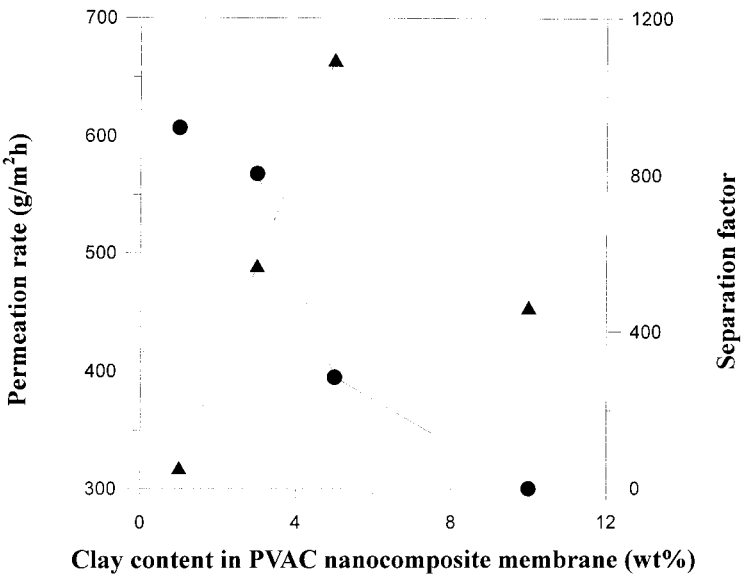

Figure 6 Effect of clay content on vapor-permeation performances of 90 wt % aqueous ethanol solutions through PVAC nanocomposite membranes: (●) permeation rate; (▲) separation factor.

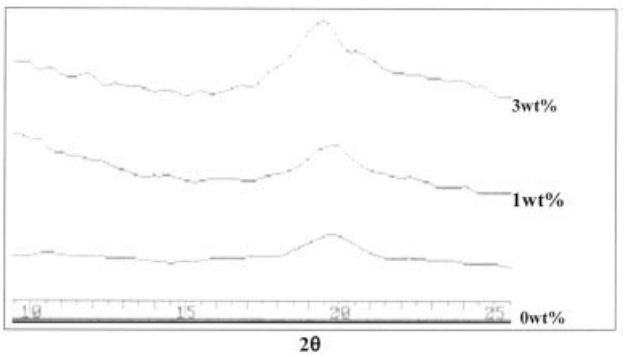

Figure 7 X-ray patterns of PVAC nanocomposite membranes.

RESULTS AND DISCUSSION

The purpose of this article was to investigate the structure of PVAC nanocomposite membranes and the effect of clay contents on the molecular barrier (oxygen and water vapor) properties. Moreover, the effects of the clay content on the vapor-permeation performances of an aqueous ethanol solution through the PVAC nanocomposite membranes were also investigated.

Characterization of PVAC nanocomposite membranes

The effects of the clay contents on the structure of the PVAC nanocomposite membranes were characterized using XRD diffraction measurements. The XRD data are collected in Figure 1. The figure shows that all PVAC nanocomposite membranes lack of any diffraction peak in 2θ = 2–10° as opposed to the diffraction peak at 2θ = 7..2°for clay (PK-805), indicating the possibility of having exfoliated silicate layers of clay dispersed in the PVA matrix. The representative FTIR spectra of the PVAC nanocomposite membranes are shown in Figure 2. Comparison of spectra (a) and (b) shows that a new absorption peak at 1042 cm^{-1}, which corresponds to (Si—O) in the clay, appeared in spectra (b). In addition, as the clay content increased, the intensity of the absorption peak at 1042 cm^{-1} became stronger in the FTIR spectra of the PVAC nanocomposite membranes. TEM was used to directly view the hybrid structure of the PVAC nanocomposite membranes. A typical TEM image is shown in Figure 3 for the 10% clay-content nanocomposite. It reveals that the silicate layers of the clay are exfoliated in the PVA matrix. In addition, the TGA curves for the thermal degradation of the PVAC nanocomposite membranes are shown in Figure 4. It shows that the loss of mass of the PVAC materials occurred above 300°C. In the presence of clay, the onsets of the loss of mass of the PVAC materials are lower than those of the pure PVA, that is, the heat stability of PVAC nanocomposite materials is higher than that of the pure PVA.

TABLE I
Effect of Clay Content on the Surface Roughness of PVAC Nanocomposite Membranes

Nanacomposite membranes	R_z (nm)	R_a (nm)	R_{ms} (nm)
PVA	29.400	2.175	2.751
PVAC1	44.617	3.350	5.225
PVAC3	127.40	12.081	15.310
PVAC5	94.432	14.209	16.808
PVAC10	155.81	14.703	19.623

R_a, average plane roughness; R_{ms}, square mean roughness; R_z 10 points mean plane roughness.

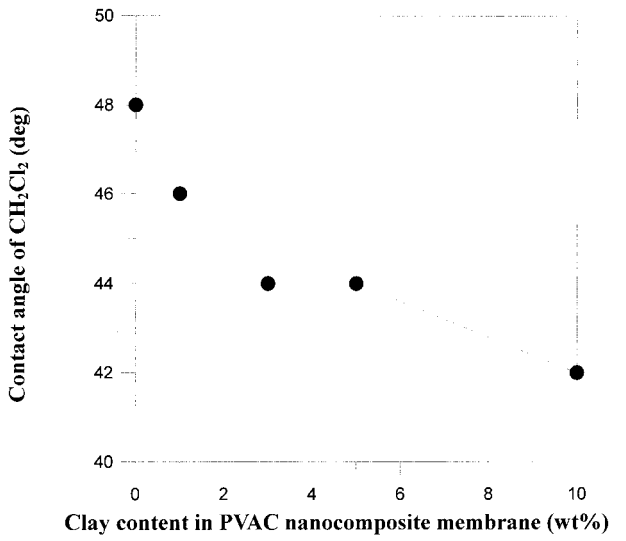

Figure 8 Effect of clay content on the surface contact angle of CH_2Cl_2.

Molecular barrier properties of the PVAC nanocomposite membranes

The molecular barrier properties of the PVAC nanocomposite membranes were studied by measurements of the oxygen and water-vapor permeability, as shown in Figure 5. It shows that the oxygen permeability and the water vapor permeation rate decreases with an increasing clay content of 1–3 wt % in the PVAC nanocomposite membranes. These phenomena might be due to that the barrier properties of the nanolayer of clay dispersed in the PVAC nanocomposite membranes result in that the tortuosity of the diffusion pathway of oxygen and water vapor increases. When the clay content in the PVAC nanocomposite membranes is higher than 5 wt %, the oxygen and water-vapor permeability increased. These phenomena might be due to that microphase separation forms between the organic polymer (PVA) and inorganic material (clay).

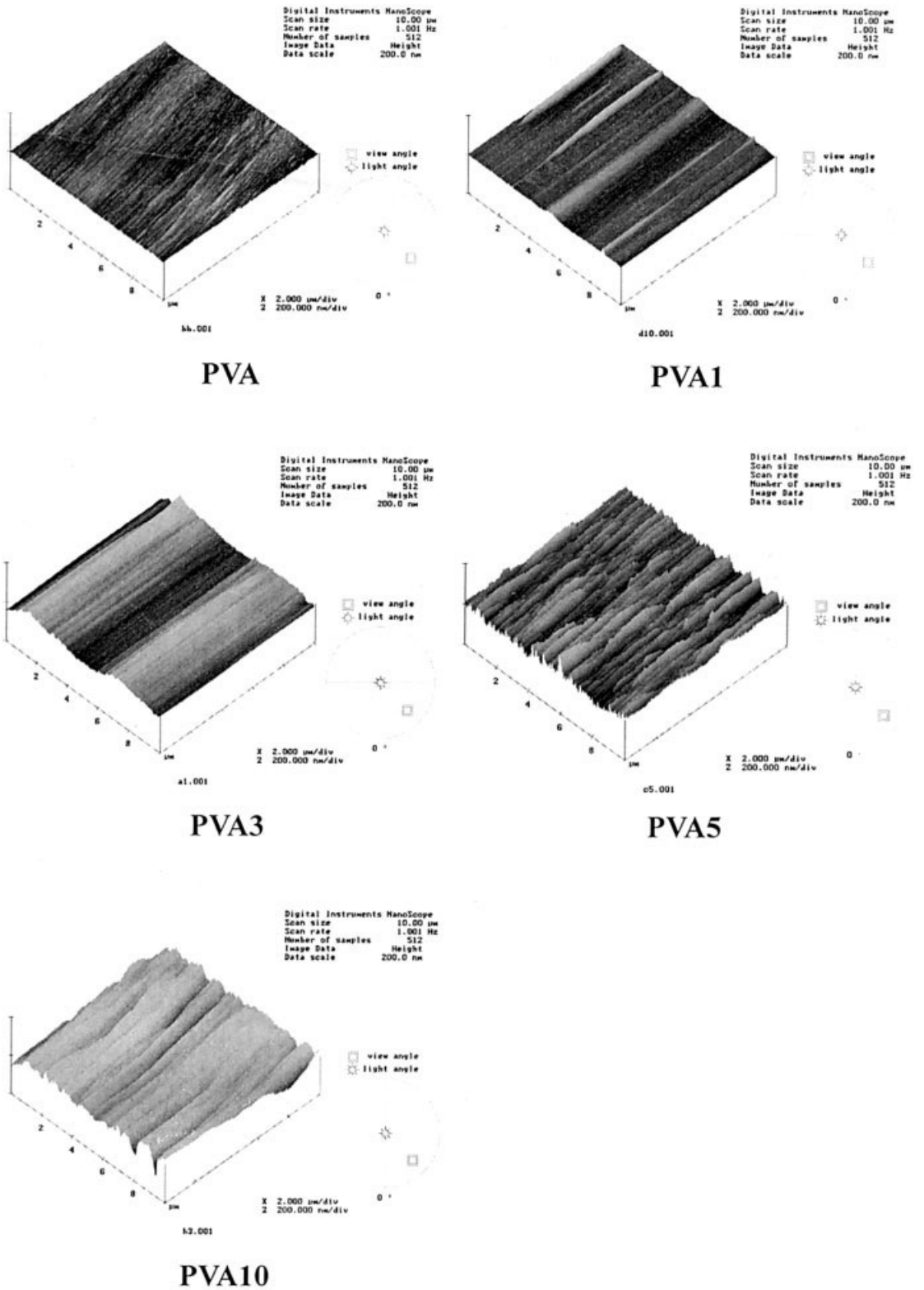

Figure 9 AFM 3-D images of the surface of the PVAC nanocomposite membranes.

Effect of clay content on vapor-permeation performance

The effect of the clay content on the permeation rates and separation factors for vapor permeation of 90 wt % aqueous ethanol solutions through PVAC nanocomposite membranes are shown in Figure 6. The figure shows that the permeation rate decreases and the separation factor increases as the clay content in-

TABLE II
Vapor-permeation or Pervaporation Performances of the Modified PVA Membranes for 90 wt % Aqueous Ethanol Feed Solution

Membrane	Separation method	Permeation rate ($g\ m^{-3}\ h^{-1}$)	Separation factor	Reference
PVAC3	VP	57.0	58.0	This work
PVAC5	VP	39.0	112.0	This work
PVA crosslinked with citric acid	PV (30°C)	84	91	8
PVA/PAA blend	PV(90°C)	32.8	12.2	9
PVA-*p*-N4	VP(25°C)	88	94	10
PVA-*p*-N4	PV(25°C)	420	13.5	10
PVA–MCA5(H)	PV(40°C)	39.5	116.5	11
PVA–MCA(Na)	PV(40°C)	39.6	107.7	11

creases. However, the separation factor decreases sharply while the clay content is higher than 5 wt % in the PVAC nanocomposite membranes. These phenomena might be due to that the crystallinity of the membrane increases with an increasing clay content in the PVAC nanocomposite membranes. Thus, the resistance of the molecular diffusion through the PVAC nanocomposite membranes increases, resulting in the permeation rate decrease.

X-ray diffraction patterns are shown in Figure 7. The figure shows that the peak intensity at $2\theta = 20°$ increases as the clay content in the PVAC nanocomposite membranes increases. This observation (Fig. 7) corresponds very well with the results indicated in Figure 6. In addition, the CH_2Cl_2 contact angle of the PVAC nanocomposite membranes also shows that the clay content increases, resulting in the contact angle decrease (Fig. 8). This implies that the hydrophilicity and the degree of swelling of the PVAC membranes decreases with an increasing clay content; thus, the permeation rate decreases as the clay content increases. Furthermore, it is widely accepted that the separation performance of the membranes are strongly related to their structure. Therefore, it is reasonable to expect that the membrane structure for the pure PVA membranes and the PVAC membranes would be different.

To further evaluate the effect of the clay content on the surface structure of PVAC membranes, in the present work, we used atomic force microscopy (AFM) to examine the membrane surface structure. The values of the surface roughness and AFM photographs are shown in Table I and Figure 9, respectively. It can be seen that the membrane-surface structures for the PVA membrane and PVAC membrane are different, which might be responsible for the difference in the vapor-permeation performance presented in Figure 6. The figure shows that the surface roughness of the PVA membrane is lower than that of the PVAC membrane. As a result, the effective vapor-permeation membrane area increases with an increasing membrane roughness. Thus, the separation factor increases with the clay content in the range of 1–5 wt %. Nevertheless, the separation factor decreases sharply when the clay content is higher than 5 wt % in the PVAC nanocomposite membranes. These results might be due to that the comparability of the organic/inorganic hybrid material decreases, resulting in microphase separation during the membrane-formation process. Furthermore, compared with the vapor-permeation or pervaporation performances of the modified PVA membranes for a 90 wt % aqueous ethanol feed solution listed in Table II, the PVAC nanocomposite membranes showed a significant improvement.

CONCLUSIONS

In this article, an organic/inorganic hybrid nanocomposite membrane having exfoliated silicate layers of clay dispersed in the PVA matrix was successfully prepared. The heat stability of the PVAC nanocomposite materials is higher than that of pure PVA. The oxygen permeability and the water-vapor permeation rate decreases with an increasing clay content in the PVAC nanocomposite membranes. The surface roughness of the PVA membranes is lower than that of the PVAC membranes. The permeation rate decreases and the separation factor increases as the clay content increases.

References

1. Huang, R. Y. M.; Yeom, C. K. J Membr Sci 1990, 51, 273.
2. Ruckenstein, E.; Liang, L. J Membr Sci 1996, 110, 99.
3. Miyata, T.; Iwamoto, T.; Uragami, T. J Appl Polym Sci 1994, 51, 2007.
4. Uragami, T.; Takigawa, K. Polymer 1990, 31, 668.
5. Vaia, R. A.; Janda, K. D.; Kramer, E. J.; Giannelis, E. P. Macromolecules 1995, 28, 8080.
6. Giannelis, E. P. Adv Mater 1996, 8, 29.
7. Teng, M. Y.; Lee, K. R.; Fan, S. C.; Liaw, D. J.; Huang, J.; Lai, J. Y. J Membr Sci 2000, 164, 241.
8. Burshe, M. C. Sep Pur Technol 1997, 12, 145.
9. Zhu, Y.; Chen, H. J Membr Sci 1998, 138, 123.
10. Lee, K. R.; Chen, R. Y.; Lai, J. Y. J Membr Sci 1992, 75, 171.
11. Kang, Y. S.; Lee, S. W.; Kim, U. Y.; Shim, J. S. J Membr Sci 1990, 51, 215.